JACS
JOURNAL OF THE AMERICAN CHEMICAL SOCIETY
Article
pubs.acs.org/JACS

Two-Coordinate Co(II) Imido Complexes as Outstanding Single-Molecule Magnets

Xiao-Nan Yao,[†,#] Jing-Zhen Du,[‡,#] Yi-Quan Zhang,[§] Xue-Bing Leng,[‡] Mu-Wen Yang,[†] Shang-Da Jiang,[†] Zhen-Xing Wang,[∥] Zhong-Wen Ouyang,[∥] Liang Deng,*[,‡] Bing-Wu Wang,*[,†] and Song Gao*[,†]

[†]Beijing National Laboratory for Molecular Sciences, State Key Laboratory of Rare Earth Materials Chemistry and Applications, College of Chemistry and Molecular Engineering, Peking University, Beijing 100871, PR China

[‡]State Key Laboratory of Organometallic Chemistry, Shanghai Institute of Organic Chemistry, Chinese Academy of Sciences, 345 Lingling Road, Shanghai 200032, PR China

[§]Jiangsu Key Laboratory for NSLSCS, School of Physical Science and Technology, Nanjing Normal University, Nanjing 210023, PR China

[∥]Wuhan National High Magnetic Field Center, Huazhong University of Science and Technology, Wuhan 430074, PR China

Supporting Information

ABSTRACT: The pursuit of single-molecule magnets (SMMs) with better performance urges new molecular design that can endow SMMs larger magnetic anisotropy. Here we report that two-coordinate cobalt imido complexes featuring highly covalent Co═N cores exhibit slow relaxation of magnetization under zero direct-current field with a high effective relaxation barrier up to 413 cm^{-1}, a new record for transition metal based SMMs. Two theoretical models were carried out to investigate the anisotropy of these complexes: single-ion model and Co−N coupling model. The former indicates that the pseudo linear ligand field helps to preserve the first-order orbital momentum, while the latter suggests that the strong ferromagnetic interaction between Co and N makes the $[CoN]^+$ fragment a pseudo single paramagnetic ion, and that the excellent performance of these cobalt imido SMMs is attributed to the inherent large magnetic anisotropy of the $[CoN]^+$ core with $|M_J = \pm 7/2\rangle$ ground Kramers doublet.

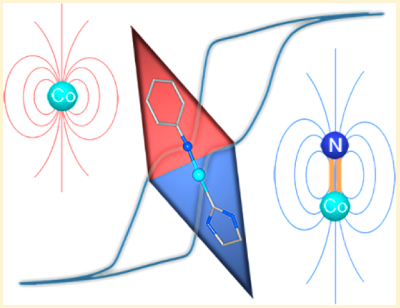

INTRODUCTION

For more than two decades, single-molecule magnets (SMMs) have attracted extensive interests to design and synthesize paramagnetic metal-containing complexes for their potential applications in the fields of high-density information storage, quantum computing and molecule spintronics.[1] Since the discovery of the first SMM Mn_{12} in the 1990s,[2] versatile metal complex-based SMMs have been reported. Among them, lanthanide SMMs stand out for their large relaxation barrier and high blocking temperature owing to their unquenched 4*f* orbital angular momentum and strong spin−orbit coupling (SOC).[3] For example, the double-decker phthalocyanine complex $[TbPc_2]^-$ has an effective relaxation barrier of U_{eff} = 230 cm^{-1}, which far exceeds those of traditional transition-metal clusters reported before.[4] Its magnetic anisotropy stems from $|M_J = \pm 6\rangle$ ground states of Tb(III) stabilized by the proper crystal field.[5] This example encouraged people to exploit the anisotropy of an independent ion. To date, though multinuclear SMMs displayed excellent performance,[6] mononuclear SMMs of Dy(III) set the record of the relaxation energy barrier of 712 cm^{-1},[7] and blocking temperature of 30 K (at the sweep rate of 200 Oe s^{-1} for hysteresis).[8] This inspired us to investigate their 3*d* transition metal counterparts. Contrary to lanthanides, the 3*d* orbitals of transition metal ions are valence orbitals and the orbital angular momentum can be readily quenched by ligand fields.[9] Thus, the second-order SOC, stemming from excited states mixing with the ground states through the spin−orbit operator, plays the major role in the magnetic anisotropy of transition metal complexes in most cases.[10] Nevertheless, low coordination number, e.g., linear two-coordinate complexes, could preserve the first-order orbital angular momentum, and significantly improve the magnetic anisotropy. For example, a series of two-coordinate homoleptic iron, cobalt, and nickel complexes with bulky amide, aryloxide, N-heterocyclic carbene (NHC), and alkyl ligation have been known to show slow relaxation of magnetization behavior.[11] Among them, a notable example is Long's Fe(I) alkyl complex $[Fe(C(SiMe_3)_3)_2]^-$, which exhibits slow relaxation of magnetization below 29 K within 1488 Hz in the absence of applied dc field and has a high effective relaxation barrier of 226 cm^{-1}, and blocking temperature up to 4.5 K, comparable to outstanding lanthanide SMMs.[11b] However, other examples do not exhibit such excellent SMM properties, which probably results from fast quantum tunneling of the magnetization (QTM).[11f,g] A potential defect of these known two-coordinate complexes is the dynamic distortion associated with the low coordination number of the metal center, the long metal−ligand σ-bond,

Received: October 23, 2016
Published: December 12, 2016

ACS Publications © 2016 American Chemical Society

DOI: 10.1021/jacs.6b11043
J. Am. Chem. Soc. 2017, 139, 373−380

which can on one hand, bring in transverse terms in the ligand-field operators, and on the other hand, readily induce unfavorable vibronic coupling.[12] Consequently, it can be expected that, in addition to a highly symmetrical ligand field, an ideal molecular design of two-coordinate transition-metal SMMs should embrace a Kramers ion and comparative rigidity of its two-coordinate core. Metal−ligand bonds with increased covalency may be an effective way to reduce vibronic coupling and enhance the magnetic anisotropy.[12]

Recently, we synthesized the two-coordinate cobalt imido complex [(IPr)CoNDmp] (**1**, Dmp = 2,6-dimesitylphenyl),[13] which represents a rare example of two-coordinate metal complexes featuring metal−ligand multiple bond.[14] Complex **1** has a near linear C(arene)−N(imido)−Co−C(carbene) alignment and a short Co−N(imido) bond (1.691(6) Å). At its ground spin state (S = 3/2), the Co−N(imido) connection has a high degree of covalency as reflected by its formal bond order of two, which arises from three fully occupied Co−N bonding interactions (one σ- and two π-bonds) and two half occupied Co−N π^*-bonding interactions. These structure features hint the unique magnetic properties of the cobalt imido complex. Accordingly, we report herein the synthesis, structure, and magnetism of two-coordinate Co(II) imido complexes that bear different NHC ligands [(NHC)CoNDmp] (**1**−**3** in Figure 1).

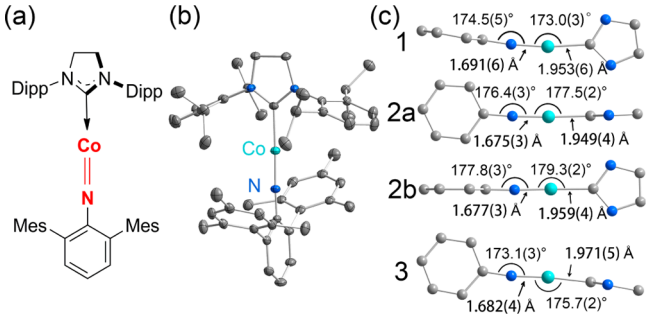

Figure 1. (a) Schematic structure of [(NHC)CoNDmp] (**3** as an example). (b) Molecular structure of **3** showing 30% probability ellipsoids and the partial atom numbering scheme. (c) Structures of the two-coordinate cores in **1**, **2a**, **2b**, and **3** with key interatomic distances and angles. Cyan, Co; blue, N; gray, C.

Magnetic studies revealed that all the three cobalt imido complexes exhibit slow relaxation of magnetization under zero applied direct current (dc) field with high effective relaxation barriers. Among them, compound **3** shows slow relaxation of magnetization at temperatures up to 50 K at 10 000 Hz, featuring the record effective relaxation barrier of 413 cm^{-1} known for transition-metal SMMs to date, and displaying magnetic hysteresis at low temperature with noticeable coercive field. Theoretical studies pointed out that the high effective relaxation barriers of these imido complexes stem from the preserved first-order orbital angular momentum (L = 2), which lead to $|M_J = \pm 7/2\rangle$ ground Kramers doublets.

RESULTS AND DISCUSSION

Sythesis and Crystal Structures. The preparation of **2** and **3** adopts a similar synthetic route as that used for **1** (Figure 2).[13] Treatment of the three-coordinate NHC-cobalt(0)-olefin complexes [(NHC)Co(CH_2=$CHSiMe_3$)$_2$] (NHC = cyIPr and sIPr), which were prepared from the one-pot reactions of $CoCl_2$ with NHC, CH_2=$CHSiMe_3$ and sodium amalgam, with one equivalent of the bulky organic azide $DmpN_3$ in n-hexane

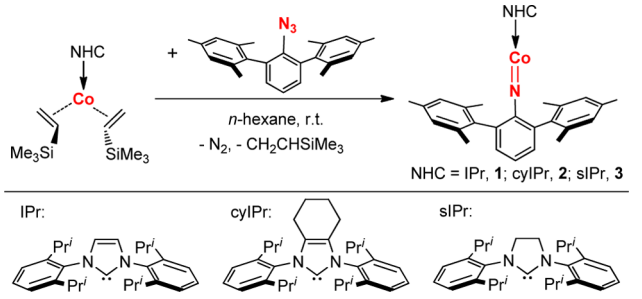

Figure 2. Synthetic route to the two-coordinate cobalt imido complexes and the designations for the NHC ligands.

led to the fast evolution of N_2 and the concomitant precipitation of the desired two-coordinate Co(II) imido complexes [(cyIPr)CoNDmp] (**2**) and [(sIPr)CoNDmp] (**3**). When gas evolution ceased, simple filtration affords **2** and **3** as yellow brown crystalline solids in 71% and 82% yields, respectively. Complexes **1**−**3** are air-, moisture-, and heat-sensitive. They show slow decomposition in solution phase at room temperature, but their solid samples can be kept at −30 °C under inert atmosphere for months without noticeable decomposition. The absorption spectra of **1**−**3** measured in benzene (Figures S4 and S5) share four intense bands in the ultraviolet−visible region (around 300, 380, 430, and 500 nm), and three broad weak bands in the near-infrared region (around 650, 850, and 1500 nm). These absorption bands are tentatively assigned as charge-transfer bands and ligand field transitions of two-coordinate Co(II) ion, respectively.[9]

Single crystals of **2** and **3** were grown from their saturated diethyl ether and tetrahydrofuran solutions, respectively, at −30 °C. X-ray diffraction studies unambiguously established the structures of **2** and **3** as two-coordinate NHC-Co-imido complexes. The unit cell of **2** contains two crystallographically independent molecules, **2a** and **2b**, whereas that of **3** has one. In analogue to **1**,[13] the crystal structures of **2** and **3** have the Co−Co separations longer than 9 Å and no arene−arene π-interaction. Figure 1b shows the structure of **3** as the representative. The structures of **2a** and **2b** are shown in Figures S2 and S3, respectively. The four molecules (**1**, **2a**, **2b**, and **3**) share the common structural features of the vertical alignment of the NHC plane toward the core arene plane of the imido ligand, near linear C(arene)−N(imido)−Co−C(carbene) alignment (Figure 1c), and short Co−N(imido) distances (1.691(6), 1.675(3), 1.677(3), and 1.682(4) Å for **1**, **2a**, **2b**, and **3**, respectively). These Co−N(imido) distances locate on the long end of Co−N(imido) distances of the reported low-coordinate cobalt terminal imido complexes,[15] and are apparently shorter than the Co−N(amido) bonds in two-coordinate cobalt(II) amido complexes (1.84−1.91 Å),[12,13] suggesting the high covalency of the CoN cores. The C(arene)−N(imido) bonds distances in **1**, **2a**, **2b**, and **3** (1.343(9), 1.343(5), 1.338(5), and 1.330(5) Å, respectively) are comparable to each other and are typical of arylimido fragments involving electron delocalization. The Co−C(carbene) distance in **3** (1.971(5) Å) is slightly longer than those in **1**, **2a** and **2b** (1.953(6), 1.949(4) and 1.959(4) Å, respectively). These structural differences could be related to the different steric property of the NHC ligands[16] as the long C−C backbone in sIPr yields a more compressed space between its Dipp groups over those in IPr and cyIPr, and hence can render more severed steric repulsion between its flanking

DOI: 10.1021/jacs.6b11043
J. Am. Chem. Soc. 2017, 139, 373−380

Dipp groups and the Mes groups on Dmp. In addition, crystal packing force might also be a contributing factor. Taken together, the structure data indicate the high covalency of the CoN motifs in these cobalt imido complexes, and the subtle but discernible geometrical difference of their C(arene)−N(imido)−Co−C(carbene) alignments.

Magnetic Characterization. The variable temperature dc magnetic susceptibility data for the polycrystalline samples of **1**−**3**, which were collected under an applied dc field of 1000 Oe between 2 and 300 K (Figure 3a, and Figures S16 and S17),

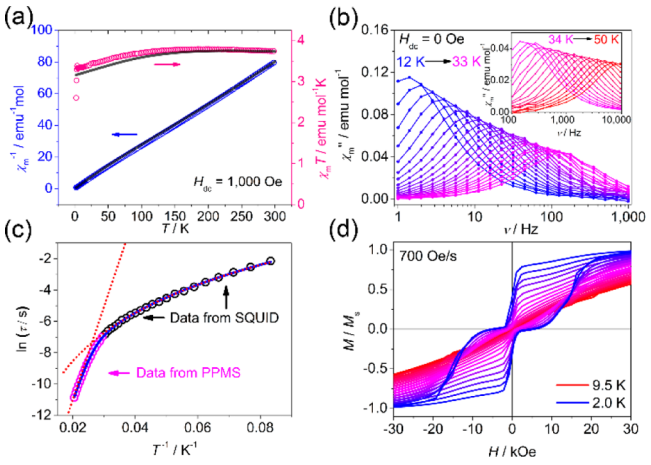

Figure 3. Magnetic properties of [(sIPr)CoNDmp] (**3**). (a) Temperature dependence of $\chi_m T$ (red) and $1/\chi_m$ (blue) values between 2 and 300 K; gray lines correspond to ab initio calculations CASPT2 using MOLCAS 7.8 program package. (b) Frequency dependence of out-of-phase alternative current (ac) susceptibilities (χ_m'') for **3**. (c) ln τ versus T^{-1} plot under 0 Oe dc field. The blue solid curve corresponds to the fit to the dual-process, and the dot lines are their individual contributions. (d) Variable-field magnetization data for **3** at the sweep rate of 700 Oe s^{-1} under 2−9.5 K.

indicated large $\chi_m T$ values at room temperature (3.86, 3.72, and 3.74 emu K mol^{-1}, respectively), far exceeding the spin-only $\chi_m T$ value of 1.875 emu K mol^{-1} for an $S = 3/2$ ion. Such large $\chi_m T$ values are typical of two-coordinate cobalt(II) species with strong spin−orbit coupling,[9,17] indicating the retention of the orbital angular momentum in **1**−**3** despite the high covalency of their CoN cores. On cooling, the $\chi_m T$ value of **1** decreases slowly and reaches 2.80 emu K mol^{-1} at 2 K, whereas, the $\chi_m T$ values of **2** and **3** slightly increase to maximum, then gradually decrease, indicating prominent magnetic anisotropy.[11a,b,12] Notably, the $\chi_m T$ of **3** shows a steep drop at 3.5 K and reaches 2.60 emu K mol^{-1} at 2 K. The abrupt change probably results from the blocking of magnetic moments and this is verified by hysteresis loops (vide infra). Low-temperature magnetization data for the three complexes collected under 1−5 T dc field (Figures S18−S20) indicated that their ground Kramers doublets may be the only populated states under low temperature.[11b] The magnetic saturation at 2 K (M_{sat} = 2.51, 2.41, and 2.46 $N\beta$ for **1**−**3**, respectively) is lower than the 3 $N\beta$ for a spin-only $S = 3/2$ ion, suggesting prominent magnetic anisotropy in these complexes.[11a] Fitting these data to the spin Hamiltonian $\mathbf{H} = \mu_B \mathbf{g}\cdot\mathbf{B}\cdot\mathbf{S} + D[\mathbf{S}_z^2 - S(S+1)/3] + E[\mathbf{S}_x^2 - \mathbf{S}_y^2]$, where D and E are the axial and rhombic anisotropy parameters, respectively, gave no reasonable results. This was expected because the precondition of the spin Hamiltonian is the quenched first-order orbital angular momentum.[1a]

Temperature and frequency dependence of alternative current susceptibility measurements revealed that all the three complexes show slow magnetic relaxation under zero applied dc field (Figures 3b and S21−S45). As shown in Figures 3b, S24 and S34, under zero applied dc field and an oscillating field H_{ac} = 3 Oe within 1−10 000 Hz, the out-of-phase ac susceptibility (χ_m'') signals versus frequency (ν) of **1**−**3** show their maxima in the temperature ranges 5−35 K, 3−42 K, and 12−50 K, respectively. For **1**, the QTM is prominent at low temperature as indicated by the temperature dependence ac susceptibilities (Figures S21 and S22) but the tunneling frequency is smaller than the lower limit of our measurement (1 Hz). Complex **2** has a similar behavior under a zero dc field (Figures S31−S34). However, the presence of 1500 Oe field notably suppresses the QTM at low temperature (Figures S25−S29 and S35−S39). For **3**, peaks of χ_m'' are observed from 12 K to as high as 50 K in the whole frequency range, suggesting the QTM is not obvious (Figures 3b and Figure S41−S45). Relations between the relaxation times (τ) and temperatures (T) are obtained through the generalized Debye model (Figures 3c, S30 and S40). In consideration of the ln τ vs T^{-1} plots are bent at the relatively lower temperature, relaxation processes other than Orbach process may play a part. We notice here the QTM-caused temperature-independent χ_m'' peaks are not observed in the $\chi_m''-\nu$ plots (Figures 3b, S24, S29, S34 and S39). Thus, the QTM process are not included in our fitting in order to avoid overparametrization. On the other hand, counting the direct process in the fitting for **1** and **3** gives no reasonable results. Thus, we consider here Orbach and Raman processes for **1** and **3**; direct, Orbach and Raman processes for **2**, using the equation

$$\tau^{-1} = \tau_0^{-1}\exp(-U_{eff}/kT) + CT^n \quad (1)$$

and

$$\tau^{-1} = AT + \tau_0^{-1}\exp(-U_{eff}/kT) + CT^n \quad (2)$$

,respectively. The best fits are listed in Table 1, with quite large effective energy barriers and pre-exponential factors τ_0 values in the typical range of 10^{-12} to 10^{-7} s of SMMs.[1,7,8,10b,11b,c,g,18] It is worth noting that the barrier of 413 cm^{-1} of **3** is the highest effective relaxation barrier for transition-metal SMMs reported to date, and even much higher than most lanthanide SMMs.[3]

Table 1. Parameters of Multiprocess Fits for Complex 1−3

	1		2		3
	0 Oe	1.5 kOe	0 Oe	1.5 kOe	0 Oe
U_{eff} (cm^{-1})	297	317	288	308	413
τ_0 (s)	7.5×10^{-11}	4.6×10^{-11}	8.4×10^{-10}	8.9×10^{-10}	1.2×10^{-10}
A (s^{-1} K^{-1})	/	/	3.0	0.2	/
C (s^{-1} K^{-n})	0.016	0.0026	0.014	1.7×10^{-5}	1.5×10^{-4}
n	3.78	4.26	3.26	5.12	4.43

DOI: 10.1021/jacs.6b11043
J. Am. Chem. Soc. 2017, 139, 373−380

The exponent of the Raman process n falls in the range of reported examples,[10b,19] with one problem that for complex **2**, the n value obtained under zero dc field (3.26) has a large discrepancy with the value obtained under 1.5 kOe (5.12). That should not have happened because Raman process is field-independent. This unusual phenomenon may be ascribed to two aspects: (a) the QTM process not included in the fitting for the reason stated above, and (b) complication of the relaxations caused by the two different molecules in one asymmetric unit.

The high temperature under which slow magnetic relaxation is observed on **3** and its high effective relaxation barrier also hint the existence of magnetic blocking. To verify the conjecture, its variable-field magnetization curves have been recorded (Figures 3d and S50). Indeed, the measurements on the powder sample of **3** at 2 K with the sweeping rate of 700 Oe s^{-1} revealed a butterfly shaped magnetic hysteresis loop with non-negligible coercive field of 4600 Oe in a commercial available SQUID.[20] As the temperature rises, the hysteresis loops close gradually and vanish at about 9.5 K. The large step around 0 Oe is attributed to the weak but still existing QTM between the lowest Kramers states. Lowering the sweep rate to 100 and 50 Oe s^{-1}, hysteresis loops with the noticeable coercive field could still be observed (~340 Oe at the rate of 50 Oe s^{-1}) though the highest blocking temperatures decrease correspondingly (Figure S50). For comparison, the coercive field in the reference[10b] vanishes under the sweep rate of 200 Oe s^{-1}. In addition to **3**, both **1** and **2** exhibit magnetic hysteresis loops but with much smaller loop-opening due to the more pronounced QTM process (Figures S46–S49).

Theoretical Analysis. In order to understand the electronic structure and magneto-structural correlation of these complexes, ab initio calculations with CASPT2 method using MOLCAS 7.8 program package[21] were performed on four model structures extracted from the three complexes (**1′**, **2a′**, **2b′**, and **3′**, the same as the ones in Figure 6a). At the beginning, we treated **1**–**3** simply as Co(II) mononuclear SMMs with the ground spin state of S = 3/2, and all spin electrons localized on the Co(II) ion. In this case, the pesudo linear ligand field helps to preserve the first-order orbital angular momentum of the Co(II) ion by maintaining degeneracy of d_{xy} and $d_{x^2-y^2}$ orbitals.[11b] Comparisons between experimental and calculated magnetic susceptibilities are shown in Figure 3a. Good agreements are met, indicating the obtained electronic structures of the complexes may be reasonable. The calculated four lowest Kramers doublets (KDs) and the anisotropic g factors of the ground KDs are listed in Table S3. The energy gaps between the ground and the first excited KD are ~280 cm^{-1}, corresponding to the large relaxation barriers obtained from ac magnetic measurements, while there is no such large difference between **3′** and the other complexes as experimental results have shown. ORCA 3.03 calculations[22] with seven electrons in the ten Co 3d+3$\acute{d}$-based orbitals and difference-dedicated configuration interaction (DDCI3)[23] on top of the CAS(7,10) reference states were also carried out. Similar results were obtained (Table S4), but the energy levels of the first excited KDs show obvious difference among **1′**–**3′** compared with CASPT2. What interests us most is the role that Co═N multiple bond plays in these excellent SMMs. The Co═N bond lengths here are 1.68–1.69 Å, much shorter than a typical Co–N single bond of 1.84 to 1.91 Å.[9] To investigate the influence of Co═N bond length, we recalculated the electronic structures of **2a′** with different Co–N distances while keeping other structural parameters unchanged (Figure 5 and Table S5). When the length of Co═N multiple bond increases

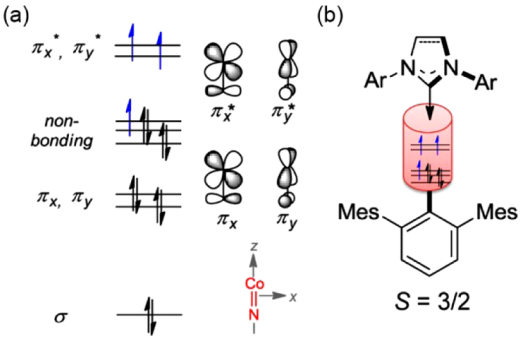

Figure 4. Bonding description for the two-coordinate NHC-cobalt-imido complex. (a) Qualitative molecular orbital description of the frontier orbitals in **1**. (b) Schematic representation of the $[CoN]^+$ core with a ground spin-state S = 3/2 by viewing the CoN moiety as a whole.

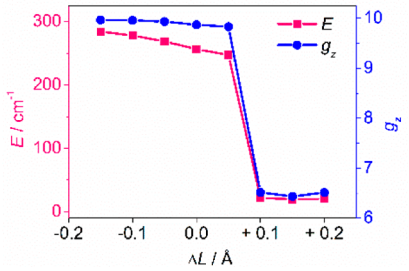

Figure 5. Calculated energy levels of the first excited KDs (E) and g_z of the ground states of **2a′** with Co–N distance changes (ΔL) using DDCI3 method on top of the CAS(7,10) reference states.

0.05 Å, a slight energy decrease of the first excited KD is found. At the same time, g_x and g_y of the ground KD grow by ten times, giving a less axial ground state. However, when another 0.05 Å is lengthened, the energy level drops dramatically to only 21.8 cm^{-1}, and the g factors become much less anisotropic. Further lengthening the bond does not make big changes. Moreover, we also explored the case of shorter Co–N distances (Figure 5 and Table S5), but no remarkable changes were observed. These amazing results indicate that the short Co═N bond does play an important role in maintaining large magnetic anisotropy in SMMs.

Considering their unique structure features compared with the traditional SMMs with only metal–ligand ionic or single bonds,[3,11c,g,18,24] we also investigated another possible situation, in which the electron spins are delocalized on the adjacent N atom through the Co═N double bond. In other words, the CoN core can be treated as a whole with the total spin of 3/2, and the uniaxial anisotropies of **1**–**3** are from strongly magnetically coupled CoN core.[25] In this case, the CoN unit has a positive charge, and the molecule can be viewed as $[NHC]^0[CoN]^+[Dmp]^-$. From molecular orbital theory, the three near-degenerate nonbond orbitals may be constituted by the Co $3d_{\pm 2}$ and Co 4s orbitals, filled with three electrons (Figure 4a). This leads to a preservation of orbital angular momentum with L = 2 and produces a uniaxial magnetic anisotropy. Further, ab initio calculations using Orca 3.03[22] were conducted on the model structures **1′**, **2a′**, **2b′**, and **3′** (Figure 6a) at their high-spin state (S = 3/2). As shown in

DOI: 10.1021/jacs.6b11043
J. Am. Chem. Soc. 2017, 139, 373–380

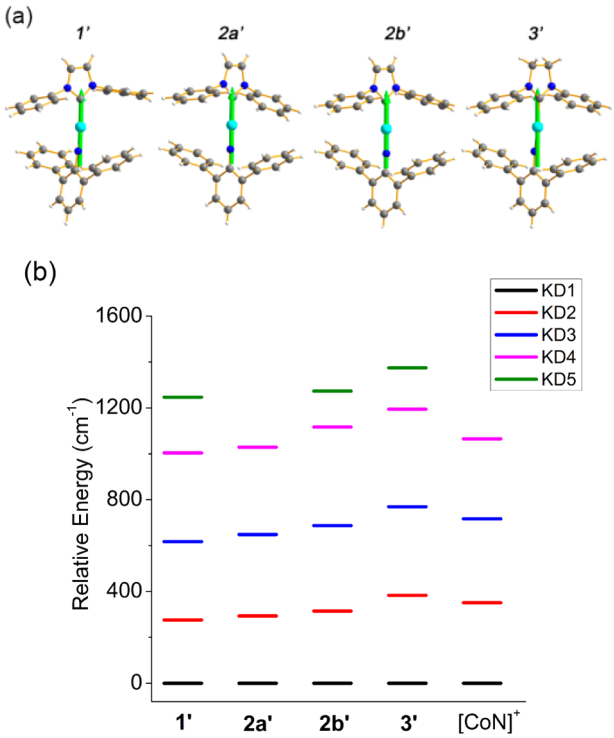

Figure 6. Geometry structures and calculated results of the model complexes **1′**−**3′** and $[CoN]^+$ at their $S = 3/2$ states. (a) Orientations of the local main magnetic axes of the ground Kramers doublets on **1′**−**3′**. The structures were extracted from the crystal structure data of **1**−**3**. Cyan, Co; blue, N; gray, C, white, H. (b) Calculated relative energy levels of the lowest Kramers doublets for **1′**−**3′** and $[CoN]^+$ at their $S = 3/2$ states.

Figure 6b and Table S7, all the spin−orbit energy levels for **1′**−**3′**, which were established by the DDCI3 on top of the CAS(9, 6) reference states calculations,[26] also feature very large energy separations of the ground and the first excited Kramers doublets (275.6, 292.9, 314.7, and 383.1 cm^{-1}, respectively). What is more, the gaps of the ground to the first excited state agree much better with the corresponding magnetic relaxation barriers of **1**−**3** obtained from ac susceptibility measurements (297, 288, and 413 cm^{-1}, respectively), supporting the molecular origin of the dynamic magnetic behavior of **1**−**3**. To further probe the nature of the magnetic anisotropy of the cobalt imido species, the spin−orbit energy level of the structure fragment $[CoN]^+$ with the optimized Co−N bond length of 1.65 Å at the $S = 3/2$ state was also calculated. As shown in Figure 6b, the relative energy levels of its four lowest Kramers doublets are comparable to those of **1′**−**3′**, and its calculated energy gap of the ground to the first excited state of 351.0 cm^{-1} is in the same magnitude as those of **1′**−**3′**, revealing that the inherent large magnetic anisotropy of the $[CoN]^+$ core plays a dominant role on the magnetic anisotropies of the cobalt imido species. Moreover, the theoretical calculation indicated that the spin population of Co and N is approximate 1 and 1/2, respectively. The short Co═N bond will lead to a strong exchange coupling interaction between Co and N spin centers. On the assumption that the spin electrons are well localized on Co and N as $S_{Co} = 1$ and $S_N = 1/2$, the isotropic exchange coupling constants J_{Co-N} estimated by B3LYP-BS calculations are 2641, 2892, 2830, 2762, and 1634 cm^{-1} for **1′**, **2a′**, **2b′**, **3′** and $[CoN]^+$ fragment (Table S6), respectively.[27] The extraordinary large J_{Co-N} values could produce a much different magnetic energy level from the common transition-metal exchange clusters. But for the molecule structure of Co imido complexes **1**−**3**, the real spin configurations may be the mixed states of $S_{Co} = 3/2$, $S_N = 0$ and $S_{Co} = 1$, $S_N = 1/2$. From the ab initio calculations, the ground and first excited states of **1**−**3** are well separated Kramers doublets with nearly well-defined M_J values, namely the Ising state with $M_L = 2$ (vide infra). The unique electronic structure makes $[CoN]^+$ be reasonable to be treated as a whole paramagnetic ion in the formation of SMMs. In fact, scientists have found some strong ferromagnetic coupled transition metal-radical compounds,[28] but they show no obvious slow relaxation of magnetization.

Thus, we can say that the large magnetic anisotropy of the $[CoN]^+$ core, which comes mainly from Co atom, coupled with N by a multiple bond, is an inherent property of $[CoN]^+$. This resembles that of the lanthanide SMMs and endows all the three complexes **1**−**3** large magnetic anisotropies despite their structural differences (vide supra). The calculated local *g*-tensors of the ground Kramers doublets of **1′**−**3′**, and $[CoN]^+$ are strongly axial (Table S8). On the basis of the ground state spin $S = 3/2$ and the calculated g_z values (10.614, 10.827, 10.887, 11.323, 10.287 for **1′**, **2a′**, **2b′**, **3′**, and $[CoN]^+$, respectively), which approach that expected for a pure $|M_J = \pm 7/2\rangle$ state of $g_z = 10$ ($S = 3/2$, $L = 2$, $J = 7/2$), one can get $g_J = 10/7$ and the $(\chi_m T)_{300\ K} = 4.02$ emu K mol^{-1}. The latter value accords with the experimental $(\chi_m T)_{300\ K}$ values of **1**−**3** (ca. 3.8 emu K mol^{-1}).[29] Thus, it is proposed that in the $[CoN]^+$ core, only orbital angular momentum of $M_L = \pm 2$ are preserved and the Kramers doublet $|M_J = \pm 7/2\rangle$ could be the ground Kramers doublet of these $[CoN]^+$ based SMMs, which is consistent with the orbital analysis of Figure 4a that the Co $3d_{\pm 2}$ orbital momentum may be preserved in the compounds. On the other hand, the first excited Kramers doublets given in Figure 6b correspond to $|M_J = \pm 5/2\rangle$ states, and all other doublets are mixed states that are difficult to identify with M_J values. However, it is worth noting that even though the $[CoN]^+$ core and its short Co═N bond play a very important role in maintaining large magnetic anisotropy, there are other factors that could also influence it. For example, the optimized $[CoN]^+$ fragment has the shortest Co═N bond (1.65 Å), but the smallest g_z value. The same thing also happens between **2** and **3**. This means the specific coordination environment, especially the charge distribution on NHC ligand for **1**−**3**, could probably make a difference on the magnetic anisotropy of these complexes. Thus, comparison of the magnetic anisotropy between different complexes should be carried out with great care.

Consistent with the Ising state being the ground Kramers doublets and the existence of the very large zero-field splitting in the ground multiplets, the high-field and high-frequency electron paramagnetic resonance (HFEPR) spectra of the solid samples of **1**−**3** in 4.2−20 K are found EPR silent (Figure S52−S54).

■ CONCLUSIONS

We found that two-coordinate cobalt imido complexes with NHC ligation in the form of [(NHC)CoNDmp] exhibit slow magnetic relaxation and blocking at relative high temperature, which represents a new class of SMMs featuring metal−ligand multiple bond. The effective relaxation barrier of one complex, [(sIPr)CoNDmp] (**3**), is 413 cm^{-1}, which sets the record of transition-metal based SMMs. Moreover, coercive field is

DOI: 10.1021/jacs.6b11043
J. Am. Chem. Soc. 2017, 139, 373−380

observed on these cobalt imido complexes. Though the simple Co(II)-based mononuclear SMM model cannot be excluded, we tend to ascribe their high effective relaxation barriers to the inherent large magnetic anisotropy of the $[CoN]^+$ core that features the $|M_J = \pm 7/2\rangle$ ground Kramers doublet. This strategy weakens (*not eliminate*) the drawback of strong QTM of mononuclear SMMs through the introduction of strong exchange coupling. These findings may stimulate explorations on the magnetic and electronic structures of low-coordinate metal species featuring metal−ligand multiple bonds, and lead to new opportunity in high performance SMM studies.

EXPERIMENTAL SECTION

Preparation. *General Methods.* All synthetic experiments were performed under an atmosphere of dry dinitrogen with the rigid exclusion of air and moisture using standard Schlenk techniques, or in a glovebox. All organic solvents were freshly distilled from sodium benzophenone ketyl immediately prior to use. All other chemicals were purchased from either Strem or J&K Chemical Co. and used as received unless otherwise noted. The compounds 1,3-bis(2′,6′-diisoproplphenyl)-4,5-dihydro-imidazol-2-ylidene (sIPr),[30] 2,6-dimesitylphenyl azide ($DmpN_3$),[31] and [(IPr)CoNDmp][13] were synthesized according to literature procedures. ^1H, ^{13}C, and ^{19}F NMR spectra were recorded on Agilent 400 MHz spectrometers. Chemical shifts were reported in units with references to the residual protons of the deuterated solvents for proton chemical shifts, the ^{13}C of deuterated solvents for carbon chemical shifts. Elemental analyses were performed by the Analytical Laboratory of Shanghai Institute of Organic Chemistry (CAS). Solution magnetic moments were measured by the method originally described by Evans with stock and experimental solutions containing a known amount of a $(CH_3)_3SiOSi(CH_3)_3$ standard.[32] Absorption spectra were recorded with a Shimadzu UV-3600 UV−vis−NIR spectrophotometer. IR spectra were recorded with a NICOLET AVATAR 330FT-IR spectrophotometer. Melting points were measured with samples sealed in thin-walled glass capillaries, and the nature of the samples was rechecked by ^1H NMR after the measurements. The EPR measurements were taken on a homemade spectrometer at Wuhan National High Magnetic Field Center, equipped with a pulsed magnetic field up to 30 T.[33] The data was collected without alternative field modulation and obtained directly in the absorption mode.

Preparation of cyIPr·HBF$_4$ (Scheme S1). The preparation of the imidazolium salt adopts a modified synthetic procedure described by Glorius for cyIPr·HBr.[34] *N*,*N*′-Bis(2,6-diisopropylphenyl)formamidine (120 mmol, 44.0 g) was suspended in acetonitrile (300 mL). NEt(*i*-Pr)$_2$ (145 mmol, 18.8 g, 24.2 mL) and 2-bromocyclohexanone (240 mmol, 42.8 g) were added successively and the resulting mixture was stirred at 110 °C for 6 days. Then, the volatiles were removed under reduced pressure. The residue was suspended in toluene (400 mL), to which acetic anhydride (360 mmol, 37.1 g, 34.3 mL) and 48% aqueous HBF_4 (180 mmol, 33.2 g) were added. The resulting mixture was stirred at 90 °C for 2 days. The mixture was then transferred into a separatory funnel containing CH_2Cl_2/H_2O (400 mL, 1/1 v/v). After separation of the two layers, the aqueous layer was extracted with CH_2Cl_2 (2 × 200 mL), and then the combined organic layers were washed with water (2 × 200 mL) and dried over anhydrous magnesium sulfate. The volatiles were removed under a vacuum to afford oily brown solid. The oily brown solid was washed with cold THF (200 mL) to afford cyIPr·HBF$_4$ as a white solid (43.6 g, 68%). ^1H NMR (400 MHz, $CDCl_3$, 19 °C): δ (ppm) = 8.93 (s, 1H, NC*H*N), 7.54 (t, J = 7.8 Hz, 2H, 2 × Ar−H), 7.32 (d, J = 7.8 Hz, 4H, 4 × Ar−H), 2.38−2.20 (m, 8H, 4 × $(CH_3)_2CH$, 2 × CH_2), 1.94 (br, 4H, 2 × CH_2), 1.24 (d, J = 6.8 Hz, 12H, 2 × $(CH_3)_2CH$), 1.16 (d, J = 6.8 Hz, 12H, 2 × $(CH_3)_2CH$). ^{13}C NMR (101 MHz, $CDCl_3$, 19 °C): δ (ppm) = 145.10, 135.87, 132.07, 131.99, 127.57, 124.78, 29.10, 24.70, 23.22, 21.33, 20.10. ^{19}F NMR (376 MHz, $CDCl_3$, 19 °C): δ (ppm) −152.96 (1F), −153.01 (3F). The presence of two ^{19}F NMR signals might be caused by the hydrogen-bonding of NCH···F−BF_3.

Preparation of cyIPr (Scheme S2). To a white suspension of cyIPr·HBF$_4$ (8.80 g, 16.6 mmol) in THF (80 mL) was added KH (1.00 g) and a catalytic amount of KOBu^t (5 mol %, 93 mg) at room temperature. The color of the mixture turned from white to pale yellow with bubble-releasing. The pale yellow suspension was stirred for 12 h and then filtered through Celite and concentrated under a vacuum to afford cyIPr as a pale yellow solid (6.7 g, 92%). ^1H NMR (400 MHz, C_6D_6, 19 °C): δ (ppm) = 7.32 (dd, J = 8.3, 7.0 Hz, 2H, 2 × Ar−H), 7.22 (d, J = 7.5 Hz, 4H, 4 × Ar−H), 2.98 (dt, J = 13.8, 6.9 Hz, 4H, 4 × $(CH_3)_2CH$), 2.08 (br, 4H, 2 × CH_2), 1.42 (br, 4H, 2 × CH_2), 1.33 (d, J = 6.8 Hz, 12H, 2 × $(CH_3)_2CH$), 1.21 (d, J = 7.0 Hz, 12H, 2 × $(CH_3)_2CH$). ^{13}C NMR (101 MHz, C_6D_6, 19 °C): δ (ppm) 217.50 (carbene carbon), 146.30, 136.86, 128.58, 127.23, 123.36, 28.58, 24.90, 22.75, 22.64, 21.37. Anal. Calcd for $C_{31}H_{42}N_2$: C, 84.11; H, 9.56; N, 6.33. Found: C, 84.07; H, 9.34; N, 6.23%.

Preparation of [(cyIPr)Co(η^2-vtms)$_2$] (Scheme S3). To a stirring THF (80 mL) solution of cyIPr (4.42 g, 10.00 mmol) was added $CoCl_2$ (1.30 g, 10.00 mmol) at room temperature. The color of the solution changed to dark blue immediately. After further stirring for 6 h, vinyltrimethylsilane (vtms, 4.00 g, 40.00 mmol) was added and the resulting dark blue reaction mixture was stirred for 2 h at room temperature. Freshly prepared sodium amalgam (0.46 g, 20.00 mmol Na; 70 g Hg) was slowly added to the reaction mixture at room temperature. The reaction mixture was stirred for another 16 h, during which the color changed to green gradually. The mixture was then filtered through Celite and concentrated under a vacuum to afford a green residue that was washed with *n*-hexane (15 mL) and dried under a vacuum to give [(cyIPr)Co(η^2-vtms)$_2$] as a green powder (5.96 g, 85%). Single-crystals of [(cyIPr)Co(η^2-vtms)$_2$] suitable for X-ray crystallography were obtained by slow evaporation of its Et_2O solution at room temperature. Melting point: 132−134 °C (decomposed). ^1H NMR (400 MHz, C_6D_6, 22 °C): δ (ppm) = 83.71 (br), 72.37 (br), 52.97 (br), 24.41 (br), 9.00(br), 5.80 (br), 5.59 (br), 5.31 (br), 3.76 (br), 3.37 (br), −0.30 (br), 2.64 (br), −3.60 (br), −9.71 (br), −25.53 (br). The ^1H NMR spectrum [(cyIPr)Co(η^2-vtms)$_2$] shows 15 paramagnetically shifted resonances, which is consistent with the idealized C_2 symmetry indicated by its crystal structure. Magnetic susceptibility (C_6D_6, 22 °C): μ_{eff} = 3.3(1) μ_B. Absorption spectrum (THF): λ_{max}, nm (ε, M^{-1} cm^{-1}) = 255 (30030), 645 (650), 840 (250). IR (KBr, cm^{-1}): υ = 3072 (w), 3036 (w), 2960 (s), 2867 (m), 1702 (s), 1667 (m), 1592 (w), 1446 (m), 1398 (s), 1363 (w), 1248 (w), 1179 (w), 1095 (w), 1062 (w), 933 (w), 837 (m), 803 (m), 770 (w), 753 (m), 598 (w). Anal. Calcd for $C_{41}H_{66}CoN_2Si_2$: C 70.14, H 9.48, N 3.99; Found: C 69.96, H 9.67, N 4.07%.

Preparation of [(sIPr)Co(η^2-vtms)$_2$] (Scheme S4). To a stirring THF (80 mL) solution of sIPr (3.90 g, 10.00 mmol) was added $CoCl_2$ (1.30 g, 10.00 mmol) at room temperature, the color of solution changed to dark blue immediately. After further stirring for 6 h, vinyltrimethylsilane (vtms, 4.00 g, 40.00 mmol) was added and the resulting dark blue reaction mixture was stirred for 2 h at room temperature. Freshly prepared sodium amalgam (0.46 g, 20.00 mmol Na; 70 g Hg) was slowly added to the reaction mixture at room temperature. The reaction mixture was stirred for another 16 h, during which the color changed to green gradually. The mixture was then filtered through Celite and concentrated under a vacuum to afford a green residue that was washed with *n*-hexane (15 mL) and dried under a vacuum to give [(sIPr)Co(η^2-vtms)$_2$] as a green powder (4.94 g, 76%). Melting point: 121−123 °C (decomposed). ^1H NMR (400 MHz, C_6D_6, 19 °C): δ (ppm) = 87.29 (br), 59.24 (br), 31.08 (br), 24.19 (br), 7.83 (br), 5.49 (br), 4.15 (br), 3.23 (br), −0.38 (br), −2.73 (br), −3.19 (br), −10.29 (br), −26.54 (br). The ^1H NMR spectrum [(sIPr)Co(η^2-vtms)$_2$] shows 13 paramagnetically shifted resonances, indicating its idealized C_2 symmetry. Magnetic susceptibility (C_6D_6, 19 °C): μ_{eff} = 2.9(1) μ_B. Absorption spectrum (THF): λ_{max}, nm (ε, M^{-1} cm^{-1}) = 246 (16800), 648 (340), 770 (270). IR (KBr, cm^{-1}): υ = 3040 (w), 2960 (s), 2868 (s), 1699 (s), 1589 (w), 1456 (m), 1418 (m), 1382 (w), 1362 (w), 1326 (w), 1280 (m), 1245 (m), 1120 (w), 1057 (w), 936 (w), 837 (w), 804 (m), 747 (m), 710 (w). Anal. Calcd for $C_{37}H_{62}CoN_2Si_2$: C 68.37, H 9.61, N 4.31; Found: C 68.50, H 9.78, N 4.10%.

DOI: 10.1021/jacs.6b11043
J. Am. Chem. Soc. 2017, 139, 373−380

*Preparation of [(cyIPr)CoNdmp] (**2**) (Scheme S5).* To a green suspension of [(cyIPr)Co(η^2-vtms)$_2$] (702 mg, 1.00 mmol) in *n*-hexane (30 mL) was added DmpN$_3$ (356 mg, 1.00 mmol) at room temperature. The color of the reaction mixture changed from green to yellow brown immediately with vigorous bubble-releasing and precipitation of a brown solid. After stirred for 20 min, the precipitate was collected by filtration and dried under high vacuum to furnish **2** as brown crystalline solid (588 mg, 71%). Single-crystals of **2** suitable for X-ray crystallography were obtained by cooling its saturated Et$_2$O solution at −30 °C. Melting point: 146−148 °C (decomposed). Complex **2** is air-, moisture-, and heat-sensitive. It shows slow decomposition in solution phase at room temperature, but its solid sample can be kept at −30 °C under inert atmosphere for months without noticeable decomposition. ^{1}H NMR (400 MHz, C$_6$D$_6$, 19 °C): δ (ppm) 137.02 (br), 64.29 (br), 14.72 (br), 4.57 (br), −20.67 (br), −22.84 (br), −35.85 (br), −41.48 (br), −158.90 (br). The ^{1}H NMR spectrum **2** only shows 9 paramagnetically shifted resonances. The two missing signals might be corresponding to the 5-CH$_2$−Cy and *p*-C$_6$H$_3$-Dmp, presumably due to the large oriented orbital angular momentum. Magnetic susceptibility (C$_6$D$_6$, 20 °C): μ_{eff} = 5.1(1) μ_B. Absorption spectrum (benzene): λ_{max}, nm (ε, M^{-1} cm^{-1}) = 300 (14700), 377 (11010), 430 (13520), 500 (4450), 654 (910), 855 (1080), 1503 (350). IR (KBr, cm^{-1}): υ = 2962 (s), 2866 (s), 1703 (s), 1667 (w), 1601 (w), 1446 (s), 1398 (m), 1363 (m), 1257 (w), 1176 (w), 1059 (w), 936 (w), 848 (m), 804 (m), 769 (m), 752 (m). Anal. Calcd for C$_{55}$H$_{67}$CoN$_3$: C 79.68, H 8.15, N 5.07; Found: C 79.53, H 8.24, N 5.04%.

*Preparation of [(sIPr)CoNdmp] (**3**) (Scheme S6).* To a green suspension of [(sIPr)Co(η^2-vtms)$_2$] (650 mg, 1.00 mmol) in *n*-hexane (30 mL) was added DmpN$_3$ (356 mg, 1.00 mmol) at room temperature. The color of the reaction mixture changed from green to yellow brown immediately with vigorous bubble-releasing and precipitation of a brown solid. After stirred for 20 min, the precipitate was collected by filtration and dried under high vacuum to furnish **3** as brown crystalline solid (637 mg, 82%). Single-crystals of **3** suitable for X-ray crystallography were obtained by cooling its saturated THF solution at −30 °C. Melting point: 102−104 °C (decomposed). Complex **3** is air-, moisture-, and heat-sensitive. It shows slow decomposition in solution phase at room temperature, but its solid sample can be kept at −30 °C under inert atmosphere for months without noticeable decomposition. ^{1}H NMR (400 MHz, THF-d_8, 19 °C): δ (ppm) 14.42 (br), 2.89 (br), −19.71 (br), −22.18 (br), −36.70 (br), −44.09 (br), −161.71 (br). The ^{1}H NMR spectrum **3** only shows 7 paramagnetically shifted resonances. The three missing signal might be corresponding to the NC*H*, *p*-C$_6$*H*$_3$-Dmp, and *p*-C$_6$*H*$_3$-Dipp, presumably due to the large oriented orbital angular momentum. Magnetic susceptibility (C$_6$D$_6$, 20 °C): μ_{eff} = 4.6(1) μ_B. Absorption spectrum (benzene): λ_{max}, nm (ε, M^{-1} cm^{-1}) = 298 (12870), 374 (9430), 434 (9880), 504 (4820), 928 (460), 1531 (150). IR (KBr, cm^{-1}): υ = 2961 (s), 2923 (s), 2868 (s), 1708 (s), 1602 (w), 1456 (s), 1418 (m), 1384 (w), 1363 (w), 1326 (w), 1268 (m), 1244 (w), 1061 (w), 850 (m), 804 (m), 748 (m). Anal. Calcd for C$_{51}$H$_{63}$CoN$_3$: C 78.83, H 8.17, N 5.41; Found: C 78.36, H 7.43, N 5.43%.

X-ray Crystallography. Diffraction-quality crystals [(cyIPr)Co(η^2-vtms)$_2$], **2**, and **3** were obtained from recrystallizations in Et$_2$O at room temperature, Et$_2$O at −30 °C, and THF at −30 °C, respectively. Crystals were coated with Paratone-*N* oil and mounted on a Bruker APEX CCD-based diffractometer equipped with an Oxford low-temperature apparatus. Cell parameters were retrieved with SMART software and refined using SAINT software on all reflections. Data integration was performed with SAINT, which corrects for Lorentz polarization and decay. Absorption corrections were applied using SADABS.[35] Space groups were assigned unambiguously by analysis of symmetry and systematic absences determined by XPREP. All structures were solved and refined using SHELXTL.[36] Metal and first coordination sphere atoms were located from direct-methods E-maps. Non-hydrogen atoms were found in alternating difference Fourier synthesis and least-squares refinement cycles and during final cycles were refined anisotropically. Table S1 summarizes the crystal data and summary of data collection and refinement for the complexes and Table S2 lists the key distances (Å) and angles (deg) of the cobalt imido complexes from X-ray crystal structures. Figure S1−S3 shows the molecular structures of [(cyIPr)Co(η^2-vtms)$_2$], and the two crystallographically independent molecules in the unit cell of [(cyIPr)CoNDmp].

Computational Details. To obtain the isotropic exchange coupling constants *J*, Orca 3.03 calculations[22] were performed with the popular hybrid functional B3LYP proposed by Becke[37] and Lee et al.[38] Triple-ζ with one polarization function TZVP[39] basis sets were used for all atoms, and zero order regular approximation (ZORA) was used for the scalar relativistic effect in all calculations. Tight convergence criteria were selected to ensure the results to be well converged with respect to technical parameters. For all complexes, through calculating the energies of two spin states: the high-spin state ($S_{HS} = S_{Co} + S_N$), the broken-symmetry (BS) state (flip the spins on N; $S_{BS} = S_{Co} - S_N$), the Co−N coupling constants J_{Co-N} was obtained by eq 3 deduced using the spin-projected approach.[27]

$$J_{Co-N} = \frac{E_{BS} - E_{HS}}{2} \quad (3)$$

Although B3LYP-BS method is not appropriate to calculate the exchange couplings for these systems due to the very strong magnetic anisotropy of Co, the results in Table S6 can qualitatively indicate the much strong ferromagnetic interaction between Co and N for each complex. Thus, we can consider Co−N as a whole to calculate their magnetic anisotropies.

To investigate the magnetic anisotropies of three complexes, Orca 3.03 calculations[22] were also performed with difference-dedicated configuration interaction (DDCI3)[26a] method. The spin−orbit coupling (SOC) operator used was the efficient implementation of the multicenter spin−orbit mean-field (SOMF) concept developed by Hess et al.[26b] The first CASSCF calculation with eight 3d electrons from Co^I and one 2p electron from N in six active orbitals (CAS(9, 6)) were performed on complexes **1′**−**3′**, and then DDCI3[26a] on top of the CAS(9, 6) reference states were carried out. In the calculations, the orbitals were determined for the average of 20 *S* = 3/2 and 70 *S* = 1/2 roots. All calculations were performed with triple-ζ with one polarization function TZVP[39] basis set for all atoms. Tight convergence criteria were used in order to ensure that the results are well converged with respect to technical parameters. B3LYP-BS and DDCI3 were used again to calculate the Co−N exchange coupling and the magnetic anisotropy of the [CoN]$^+$ moiety, respectively. The basis sets and the active space are the same shown above. The optimized Co−N distance by B3LYP/TZVP was 1.650 Å at its *S* = 3/2 spin state. The calculated spin−orbit energy levels of **1′**−**3′** and the [CoN]$^+$ moiety are shown in Table S7. The calculated **g** tensors of the ground states of **1′**−**3′** and the [CoN]$^+$ moiety is shown in Table S8. Figure S51 depicts the spin-density distribution of **1′**−**3′** and [CoN]$^+$ at their *S* = 3/2 state.

■ ASSOCIATED CONTENT

Supporting Information

The Supporting Information is available free of charge on the ACS Publications website at DOI: 10.1021/jacs.6b11043.

Reaction schemes, crystallographic data, UV−vis spectra, ^{1}H NMR spectra, magnetometry data, EPR spectra, calculation results and Cartesian coordinates for **1′**, **2a′**, **2b′**, and **3′** (PDF)

X-ray data (CIF)

■ AUTHOR INFORMATION

Corresponding Authors

*deng@sioc.ac.cn

*wangbw@pku.edu.cn

*gaosong@pku.edu.cn

DOI: 10.1021/jacs.6b11043
J. Am. Chem. Soc. 2017, 139, 373−380

ORCID

Shang-Da Jiang: 0000-0003-0204-9601
Bing-Wu Wang: 0000-0001-8092-5959

Author Contributions

#X.-N.Y. and J.-Z.D. contributed equally.

Notes

The authors declare no competing financial interest.

■ ACKNOWLEDGMENTS

The authors thank the financial support from National Natural Science Foundation of China (21421091, 21432001, 21290171, 21321001, 91422302 and 21571008), National Key Basic Research Program of China (2013CB933401), the National Key Research and Development Program (2016YFA0202900) and Natural Science Foundation of Jiangsu Province 398 of China (BK20151542).

■ REFERENCES

(1) (a) Gatteschi, D.; Sessoli, R.; Villain, J. *Molecular Nanomagnets*; Oxford Univ. Press: Oxford, 2006. (b) Gao, S. *Molecular Nanomagnets and Related Phenomena*; Springer: Berlin, 2015.

(2) (a) Caneschi, A.; Gatteschi, D.; Sessoli, R.; Barra, A. L.; Brunel, L. C.; Guillot, M. *J. Am. Chem. Soc.* **1991**, *113*, 5873. (b) Sessoli, R.; Gatteschi, D.; Caneschi, A.; Novak, M. A. *Nature* **1993**, *365*, 141.

(3) Woodruff, D. N.; Winpenny, R. E. P.; Layfield, R. A. *Chem. Rev.* **2013**, *113*, 5110.

(4) Ishikawa, N.; Sugita, M.; Ishikawa, T.; Koshihara, S.-y.; Kaizu, Y. *J. Am. Chem. Soc.* **2003**, *125*, 8694.

(5) Rinehart, J. D.; Long, J. R. *Chem. Sci.* **2011**, *2*, 2078.

(6) (a) Pugh, T.; Chilton, N. F.; Layfield, R. A. *Angew. Chem., Int. Ed.* **2016**, *55*, 11082. (b) Rinehart, J. D.; Fang, M.; Evans, W. J.; Long, J. R. *Nat. Chem.* **2011**, *3*, 538. (c) Rinehart, J. D.; Fang, M.; Evans, W. J.; Long, J. R. *J. Am. Chem. Soc.* **2011**, *133*, 14236. (d) Layfield, R. A. *Organometallics* **2014**, *33*, 1084.

(7) Liu, J.; Chen, Y. C.; Liu, J. L.; Vieru, V.; Ungur, L.; Jia, J. H.; Chibotaru, L. F.; Lan, Y.; Wernsdorfer, W.; Gao, S.; Chen, X. M.; Tong, M. L. *J. Am. Chem. Soc.* **2016**, *138*, 5441.

(8) (a) Chen, Y. C.; Liu, J. L.; Ungur, L.; Liu, J.; Li, Q. W.; Wang, L. F.; Ni, Z. P.; Chibotaru, L. F.; Chen, X. M.; Tong, M. L. *J. Am. Chem. Soc.* **2016**, *138*, 2829. (b) Gupta, S. K.; Rajeshkumar, T.; Rajaraman, G.; Murugavel, R. *Chem. Sci.* **2016**, *7*, 5181.

(9) Power, P. P. *Chem. Rev.* **2012**, *112*, 3482.

(10) (a) Ruamps, R.; Batchelor, L. J.; Maurice, R.; Gogoi, N.; Jiménez-Lozano, P.; Guihéry, N.; de Graaf, C.; Barra, A.-L.; Sutter, J.-P.; Mallah, T. *Chem. - Eur. J.* **2013**, *19*, 950. (b) Rechkemmer, Y.; Breitgoff, F. D.; van der Meer, M.; Atanasov, M.; Hakl, M.; Orlita, M.; Neugebauer, P.; Neese, F.; Sarkar, B.; van Slageren, J. *Nat. Commun.* **2016**, *7*, 10467. (c) Ding, M.; Cutsail, G. E.; Aravena, D.; Amoza, M.; Rouzieres, M.; Dechambenoit, P.; Losovyj, Y.; Pink, M.; Ruiz, E.; Clerac, R.; Smith, J. M. *Chem. Sci.* **2016**, *7*, 6132.

(11) (a) Zadrozny, J. M.; Atanasov, M.; Bryan, A. M.; Lin, C. Y.; Rekken, B. D.; Power, P. P.; Neese, F.; Long, J. R. *Chem. Sci.* **2013**, *4*, 125. (b) Zadrozny, J. M.; Xiao, D. J.; Atanasov, M.; Long, G. J.; Grandjean, F.; Neese, F.; Long, J. R. *Nat. Chem.* **2013**, *5*, 577. (c) Dey, M.; Gogoi, N. *Angew. Chem., Int. Ed.* **2013**, *52*, 12780. (d) Frost, J. M.; Harriman, K. L. M.; Murugesu, M. *Chem. Sci.* **2016**, *7*, 2470. (e) Gómez-Coca, S.; Aravena, D.; Morales, R.; Ruiz, E. *Coord. Chem. Rev.* **2015**, *289−290*, 379. (f) Meng, Y.-S.; Mo, Z.; Wang, B.-W.; Zhang, Y.-Q.; Deng, L.; Gao, S. *Chem. Sci.* **2015**, *6*, 7156. (g) Craig, G. A.; Murrie, M. *Chem. Soc. Rev.* **2015**, *44*, 2135.

(12) Atanasov, M.; Zadrozny, J. M.; Long, J. R.; Neese, F. *Chem. Sci.* **2013**, *4*, 139.

(13) Du, J.; Wang, L.; Xie, M.; Deng, L. *Angew. Chem., Int. Ed.* **2015**, *54*, 12640.

(14) Laskowski, C. A.; Miller, A. J. M.; Hillhouse, G. L.; Cundari, T. R. *J. Am. Chem. Soc.* **2011**, *133*, 771.

(15) (a) Dai, X. L.; Kapoor, P.; Warren, T. H. *J. Am. Chem. Soc.* **2004**, *126*, 4798. (b) Jones, C.; Schulten, C.; Rose, R. P.; Stasch, A.; Aldridge, S.; Woodul, W. D.; Murray, K. S.; Moubaraki, B.; Brynda, M.; La Macchia, G.; Gagliardi, L. *Angew. Chem., Int. Ed.* **2009**, *48*, 7406. (c) King, E. R.; Sazama, G. T.; Betley, T. A. *J. Am. Chem. Soc.* **2012**, *134*, 17858. (d) Zhang, L.; Liu, Y. S.; Deng, L. *J. Am. Chem. Soc.* **2014**, *136*, 15525.

(16) Dorta, R.; Stevens, E. D.; Scott, N. M.; Costabile, C.; Cavallo, L.; Hoff, C. D.; Nolan, S. P. *J. Am. Chem. Soc.* **2005**, *127*, 2485.

(17) Bryan, A. M.; Merrill, W. A.; Reiff, W. M.; Fettinger, J. C.; Power, P. P. *Inorg. Chem.* **2012**, *51*, 3366.

(18) Novikov, V. V.; Pavlov, A. A.; Nelyubina, Y. V.; Boulon, M.-E.; Varzatskii, O. A.; Voloshin, Y. Z.; Winpenny, R. E. P. *J. Am. Chem. Soc.* **2015**, *137*, 9792.

(19) Boulon, M.-E.; Cucinotta, G.; Luzon, J.; Degl'Innocenti, C.; Perfetti, M.; Bernot, K.; Calvez, G.; Caneschi, A.; Sessoli, R. *Angew. Chem., Int. Ed.* **2013**, *52*, 350.

(20) Ruamps, R.; Batchelor, L. J.; Guillot, R.; Zakhia, G.; Barra, A.-L.; Wernsdorfer, W.; Guihéry, N.; Mallah, T. *Chem. Sci.* **2014**, *5*, 3418.

(21) Karlström, G.; Lindh, R.; Malmqvist, P.-Å.; Roos, B. O.; Ryde, U.; Veryazov, V.; Widmark, P.-O.; Cossi, M.; Schimmelpfennig, B.; Neogrady, P.; Seijo, L. *Comput. Mater. Sci.* **2003**, *28*, 222.

(22) Neese, F. *ORCA—An Ab Initio, Density Functional and Semiempirical Program Package*, Version 3.03; 2015.

(23) Miralles, J.; Castell, O.; Caballol, R.; Malrieu, J. P. *Chem. Phys.* **1993**, *172*, 33.

(24) Mills, D. P.; Moro, F.; McMaster, J.; van Slageren, J.; Lewis, W.; Blake, A. J.; Liddle, S. T. *Nat. Chem.* **2011**, *3*, 454.

(25) (a) Hernández Sánchez, R.; Bartholomew, A. K.; Powers, T. M.; Ménard, G.; Betley, T. A. *J. Am. Chem. Soc.* **2016**, *138*, 2235. (b) Hernandez Sanchez, R.; Betley, T. A. *J. Am. Chem. Soc.* **2015**, *137*, 13949.

(26) (a) Miralles, J.; Castell, O.; Caballol, R.; Malrieu, J. P. *Chem. Phys.* **1993**, *172*, 33. (b) Heß, B. A.; Marian, C. M.; Wahlgren, U.; Gropen, O. *Chem. Phys. Lett.* **1996**, *251*, 365.

(27) (a) Noodleman, L. *J. Chem. Phys.* **1981**, *74*, 5737. (b) Noodleman, L.; Baerends, E. J. *J. Am. Chem. Soc.* **1984**, *106*, 2316. (c) Noodleman, L.; Case, D. A. *Adv. Inorg. Chem.* **1992**, *38*, 423.

(28) (a) Kahn, O.; Prins, R.; Reedijk, J.; Thompson, J. S. *Inorg. Chem.* **1987**, *26*, 3557. (b) Hicks, R. G.; Lemaire, M. T.; Thompson, L. K.; Barclay, T. M. *J. Am. Chem. Soc.* **2000**, *122*, 8077. (c) Brook, D. J. R.; Richardson, C. J.; Haller, B. C.; Hundley, M.; Yee, G. T. *Chem. Commun.* **2010**, *46*, 6590. (d) Iovan, D. A.; Betley, T. A. *J. Am. Chem. Soc.* **2016**, *138*, 1983.

(29) Kahn, O. *Molecular Magnetism*; VCH Pub.: New York, 1993.

(30) Arduengo, A. J.; Krafczyk, R.; Schmutzler, R.; Craig, H. A.; Goerlich, J. R.; Marshall, W. J.; Unverzagt, M. *Tetrahedron* **1999**, *55*, 14523.

(31) Gavenonis, J.; Tilley, T. D. *Organometallics* **2002**, *21*, 5549.

(32) (a) Evans, D. F. *J. Chem. Soc.* **1959**, 2003. (b) Sur, S. K. *J. Magn. Reson.* **1989**, *82*, 169.

(33) Nojiri, H.; Ouyang, Z. W. *Terahertz Sci. Technol.* **2012**, *5*, 1.

(34) Hirano, K.; Urban, S.; Wang, C.; Glorius, F. *Org. Lett.* **2009**, *11*, 1019.

(35) Sheldrick, G. M. *SADABS: Program for Empirical Absorption Corrections of Area Detector Data*; 1996.

(36) Sheldrick, G. M. *SHELXTL*; 1997.

(37) (a) Becke, A. D. *J. Chem. Phys.* **1993**, *98*, 5648. (b) Becke, A. D. *Phys. Rev. A: At., Mol., Opt. Phys.* **1988**, *38*, 3098.

(38) Lee, C. T.; Yang, W. T.; Parr, R. G. *Phys. Rev. B: Condens. Matter Mater. Phys.* **1988**, *37*, 785.

(39) (a) Schafer, A.; Horn, H.; Ahlrichs, R. *J. Chem. Phys.* **1992**, *97*, 2571. (b) Schafer, A.; Huber, C.; Ahlrichs, R. *J. Chem. Phys.* **1994**, *100*, 5829.

DOI: 10.1021/jacs.6b11043
J. Am. Chem. Soc. 2017, 139, 373−380